

## FLOW PREDICTIONS ABOUT THREE-DIMENSIONAL HIGH LIFT SYSTEMS

Eric Besnard\*, Orhan Kural†, and Tuncer Cebeci‡

Aerospace Engineering Department  
California State University, Long Beach

### **Abstract**

An efficient and accurate calculation method for the prediction of flows about three-dimensional high lift systems is described. The method is based on the interactive solution of the inviscid flow, boundary layer and stability/transition equations. The extension of the modified Cebeci-Smith model to three-dimensional flows is first validated for separated flows. Also, the efficiency and robustness of the method are improved by linearizing the turbulence terms in the boundary layer equations. Then, the method is applied to the calculation of lift and drag coefficients about a single element wing up to stall. Results demonstrate the ability of the method to predict three-dimensional separated flows reliably, including near stall conditions. Finally, the method is applied to multi-element wings with slat and flap deployed. Both lift and drag coefficients are well predicted, except for stall which is not captured by the method in these cases. Overall, results demonstrate the potential for using the method as a practical and efficient design tool for high lift applications.

### **1.0 Introduction**

Computational fluid dynamics (CFD) calculations are now being routinely performed with Navier-Stokes methods leading to significant savings by reducing wind tunnel testing. Over the last thirty years, progress has been so impressive that one may even say that CFD has reached its maturity.

An area that still requires further work in CFD is the development of methods for predicting the aerodynamic performance of high lift configurations. The presence of high and low

Reynolds number flows on various components of wings and significant regions of flow separation well before stall conditions makes the development of such a capability a challenging task. The required generality and accuracy of the method and, equally important, its efficiency as a design tool, introduce additional challenges.

To reach this goal, one approach consists of solving the Navier-Stokes equations with structured or unstructured grids. The solution with structured grids for high lift configurations requires an extensive grid generation effort. Also, several million points are needed to appropriately resolve the flowfield about complex three-dimensional configurations, leading to high demands on computer resources. Therefore, this approach is still inadequate in a design environment where many flow solutions are needed in a single day.<sup>3</sup> Also, the transition calculation – critical for accurate drag<sup>1</sup> and Reynolds number effect<sup>2</sup> predictions – cannot be easily incorporated into the method. The solution of the Navier-Stokes equations on unstructured grids will without any doubt be the favored approach in the longer term, especially for complex three-dimensional configurations. Its requirements in computer resources, however, are even larger than for its structured grid counterpart.

The other approach is the one based on Interactive Boundary Layer (IBL) theory in which the inviscid flow, boundary layer, and stability/transition equations are solved interactively. It has been applied successfully to two-dimensional flows<sup>1</sup>. The method is designed to provide results of similar quality to that of Navier-Stokes solutions at a cost barely exceeding that of the methods currently used in high lift design (often based on potential flow theory). As such, it provides a good compromise between the efficiency and accuracy required in a design process<sup>3</sup>. The method has been recently

---

\* Lecturer, AIAA member

† Professor

‡ Professor and Chair, AIAA Fellow

applied to two-dimensional high lift system design /optimization<sup>4</sup> and is presented here for three-dimensional configurations.

The IBL approach involves interaction between inviscid, boundary layer and stability equations. The inviscid flow is computed either by a panel method (with or without compressibility corrections), a full-potential, or an Euler method, and the viscous flow is computed by a compressible boundary layer method. The onset of the transition location is computed by the  $e^n$ -method. A previous paper<sup>5</sup> presented the method and discussed its application to single element wings with large regions of separated flow and addressed issues related to the prediction of transition. The present paper improves the speed and robustness of the method and focuses on its accuracy for high lift applications.

The calculation method is briefly described in Sect. 2. The accuracy of the three-dimensional modified Cebeci-Smith turbulence model for flows with strong adverse pressure gradient is discussed in Sect. 3. In Sect. 4, the effects that the partial linearization of the turbulence terms in the boundary layer equations have on the speed and the robustness of the method are investigated for flows with large regions of separation. Then the method is applied to the calculation of lift and drag coefficients up to stall for a single element wing in Sect. 5 and results are compared with experimental data. The case of multi-element wings is treated in Sect. 6. The paper ends with a summary of the more important conclusions.

## 2.0 Calculation method

In principle, the calculation method for three-dimensional flows is similar to its two-dimensional counterpart developed for predicting the flow about single and multi-element airfoils.<sup>1</sup> It is based on the interactive solution of the inviscid, boundary layer, and stability equations as shown in Fig. 1.

Since the method is described in more detail in other references<sup>5-7</sup>, only a brief description is included here, focusing on the recent improvements.

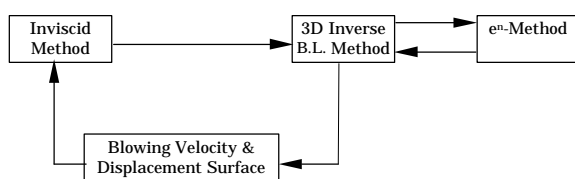


**Fig. 1. Interactive Boundary Layer method**

### 2.1 Inviscid method

The inviscid flow is computed by the higher-order Hess panel method<sup>8</sup>, which is applicable to a complete airplane configuration. In this method a general body is represented by means of a set of curved quadrilateral panels. The complete solution for a prescribed flow condition is obtained by simultaneously satisfying a condition of zero or prescribed normal velocity at a control point on each panel of the body together with a Kutta condition at each trailing edge panel. Alternatively and without loss of generality, an Euler or full potential method could be substituted for the panel method.

### 2.2 Boundary layer method

Once the velocity components are determined with the inviscid method, they are transformed into a non-orthogonal body-fitted coordinate system generated on the wing surface. The equations are solved for the upper and lower surfaces of the wing, from the stagnation line to the trailing edge and into the wake. The compressible boundary layer equations and their solution can be found in Ref. 6, and, for conciseness, only a summary corresponding to their incompressible counterpart is presented here.

#### Boundary layer equations

For a body-fitted coordinate system, these equations, with the eddy viscosity concept,  $\nu_t$ , are

Continuity Equation

$$\frac{\partial}{\partial x}(uh_2 \sin\theta) + \frac{\partial}{\partial z}(wh_1 \sin\theta) + \frac{\partial}{\partial y}(vh_1 h_2 \sin\theta) = 0 \quad (1)$$

x-Momentum Equation

$$\begin{aligned} & \frac{u}{h_1} \frac{\partial u}{\partial x} + \frac{w}{h_2} \frac{\partial u}{\partial z} + v \frac{\partial u}{\partial y} \\ & - k_1 u^2 \cot\theta + k_2 w^2 \operatorname{cosec}\theta + k_{12} uw \\ & = - \frac{\operatorname{cosec}^2 \theta}{\rho h_1} \frac{\partial p}{\partial x} + \frac{\cot\theta \operatorname{cosec}\theta}{\rho h_2} \frac{\partial p}{\partial z} + v \frac{\partial}{\partial y} \left( b \frac{\partial w}{\partial y} \right) \end{aligned} \quad (2)$$

z-Momentum Equation

$$\begin{aligned} & \frac{u}{h_1} \frac{\partial w}{\partial x} + \frac{w}{h_2} \frac{\partial w}{\partial z} + v \frac{\partial w}{\partial y} \\ & - k_2 w^2 \cot\theta + k_1 u^2 \operatorname{cosec}\theta + k_{21} uw \quad (3) \\ & = \frac{\cot\theta \operatorname{cosec}\theta}{\rho h_1} \frac{\partial p}{\partial x} - \frac{\operatorname{cosec}^2\theta}{\rho h_2} \frac{\partial p}{\partial z} + v \frac{\partial}{\partial y} \left( b \frac{\partial w}{\partial y} \right) \end{aligned}$$

Here  $x$  denotes the axial direction,  $z$  the spanwise direction, and  $y$  is normal to the surface. Also  $h$  denotes the metric coefficients,  $k$  the curvature parameters,  $\theta$  the angle between the coordinate lines  $x = \text{const.}$  and  $z = \text{const.}$ , and  $b$  ( $\equiv 1 + v_i/v$ ) contains the turbulence terms.

The corresponding boundary conditions on the body are:

$$y = 0, \quad u = 0, \quad v = 0, \quad w = 0 \quad (4a)$$

$$y = \delta, \quad u = u_e(x, z), \quad w = w_e(x, z) \quad (4b)$$

The wake is separated into upper and lower wakes, with the boundary between upper and lower wakes defined by the inviscid dividing streamline which originates at the wing trailing edge. A symmetric boundary condition in the streamwise direction and an anti-symmetric one in the crosswise direction are assumed (see Fig. 2), so that the boundary condition along the dividing streamline becomes

$$y = 0, \quad \frac{\partial u}{\partial y} = w = v = 0 \quad (4c)$$

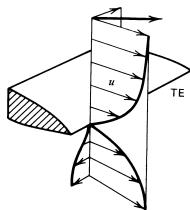


Fig. 2. Flow near wing trailing edge<sup>9</sup>

### Inverse formulation

To solve the boundary layer equations in regions of separated flow, an inverse formulation must be used. Veldman's interaction law<sup>10</sup> is employed here to couple the solutions of the inviscid and viscous flow equations and treat the external velocities,  $u_e(x)$  and  $w_e(x)$ , and the displacement thickness as unknown quantities. The external boundary condition for the boundary-layer equations are written as

$$\begin{aligned} u_e(x, z) &= u_e^o(x, z) + \delta u_e(x, z) \\ w_e(x, z) &= w_e^o(x, z) + \delta w_e(x, z) \end{aligned} \quad (5)$$

where  $u_e^o$  and  $w_e^o$  denote the inviscid velocity and  $\delta u_e$  and  $\delta w_e$  the perturbation due to the displacement thickness, which are calculated from the Hilbert integral.

For the present study, the boundary layer equations are solved in their quasi-three-dimensional form (i.e. all derivatives in the  $z$ -direction are neglected). Under this approximation, it can be shown that  $\delta w_e$  vanishes and that the expression for  $\delta u_e$  reduces to its two-dimensional flow form, so that, at a given inviscid-viscous cycle, *cyc* (a cycle is defined as a loop in Fig. 1), the perturbation velocity is given by

$$(\delta u_e)^{cyc} = \frac{1}{\pi} \int_{x_a}^{x_b} \left[ \left( \frac{d}{d\sigma} (u_e \delta_x^*) \right)^{cyc} - \left( \frac{d}{d\sigma} (u_e \delta_x^*) \right)^{cyc-1} \right] \frac{d\sigma}{x - \sigma}$$

Since  $u_e^o$  is computed from the inviscid method with the blowing velocity/displacement surface corresponding to the boundary layer solution of the inviscid-viscous cycle *cyc*-1, the contribution of the displacement surface corresponding to the previous cycle, *cyc*-1, has been subtracted from  $(\delta u_e)^{cyc}$ .

Also, as in two-dimensional separated flow calculations, the FLARE approximation is used for three-dimensional separated flows. See Ref. 6 for details.

### Transformation of the equations

The equations are then transformed using, for the independent variables,

$$d\eta = \left( \frac{u_0}{\rho_0 \mu_0 s} \right)^{1/2} \rho dy, \quad s = \int_0^x h_1 dx \quad (6)$$

where  $u_0 = u_e$  in standard mode ( $u_e$  known) and  $u_0 = u_\infty$  in inverse mode ( $u_e$  unknown), and where  $x$  and  $z$  are unchanged. For the dependent variables  $u$ ,  $v$ , and  $w$ , a two-component vector potential is introduced such that:

$$\psi = (\rho_0 \mu_0 u_0 s)^{1/2} h_2 \sin \theta f(x, z, \eta) \quad (7)$$

$$\Phi = (\rho_0 \mu_0 u_0 s)^{1/2} u_\infty / u_0 h_1 h_2 \sin \theta g(x, z, \eta) \quad (8)$$

Initial conditions are generated along the attachment line by a similar transformation, with  $u_0 = u_{xc}$ . See Ref. 6 for details.

### Solution procedure

As mentioned above, for the present study the equations are simplified using the quasi-

three-dimensional flow approximation. The resulting equations are transformed into a set of first order partial differential equations and discretized using a central difference in  $y$  and a two-point backward difference in  $x$  for second order accuracy. The system of nonlinear difference equations is then linearized with Newton's method, with the initial guesses provided by the station upstream of the point where the solution is being calculated. In the original formulation, the turbulence terms,  $b$ , stemming from Eqs. (2) and (3) are not linearized but are updated at each Newton iteration. Their partial linearization and its effects are presented in Sect. 4.

### *Turbulence model*

Turbulent flow calculations are performed using a modified Cebeci-Smith (CS) eddy-viscosity formulation<sup>11</sup> extended to three-dimensional flows. In the non-orthogonal coordinate system, inner and outer eddy viscosity expressions are given by

$$(v_t)_i = \ell^2 \left[ \left( \frac{\partial u}{\partial y} \right)^2 + \left( \frac{\partial w}{\partial y} \right)^2 + 2 \cos \theta \frac{\partial u}{\partial y} \frac{\partial w}{\partial y} \right]^{1/2} \gamma_{tr} \quad (9)$$

$$(v_t)_o = \alpha \left| \int_0^{\delta} (u_{te} - u_t^2) dy \right| \gamma_{tr} \gamma \quad (10)$$

where  $u_t^c = u^c + w^c + 2uw \cos \theta$  and the other parameters have the same definitions as for two-dimensional flows.<sup>1</sup>

The modifications of the two-dimensional CS model<sup>11</sup> are extended here to three-dimensional flows. The first improvement is to relate the parameter  $\alpha$  of Eq. (10) to a parameter  $F$  leading to

$$\alpha = \frac{0.0168}{F^{1.5}} \quad (11)$$

Here  $(1 - F)$  denotes the ratio of the production of the turbulence energy by normal stresses to that by shear stress, evaluated at the location where shear stress is maximum. The two-dimensional expression for  $F$  is used, i.e.

$$F = 1 - \beta \frac{\partial u / \partial s}{\partial u / \partial y} \quad (12)$$

where, as for two-dimensional flows,  $\beta$  is assumed to be a function of  $R_t = \tau_w / (\tau')_{\max}$ . Here  $\tau_w$  is the shear stress at the wall and  $\tau'$  is the total turbulent shear stress, evaluated at its maximum value in the boundary layer. The two-

dimensional flow expression<sup>7</sup> for  $\beta$  is assumed to be valid for three-dimensional flows.

The second modification of the original CS model consists of replacing Klebanoff's intermittency formulation with an expression valid for flows with pressure gradients. It is assumed that, for the flows of interest in the present study, the pressure gradient in the streamwise direction is much larger than that in the crosswise direction. Therefore, the expressions derived for two-dimensional flows can be extended to three-dimensional flows by applying them to the streamwise component only. See Ref. 6 for details.

The above expressions cannot be used in the wake since the inner region formulas are based on wall bounded flows. A relaxation model, similar to the one used for two-dimensional wake flows, is introduced. The eddy viscosity is written

$$v_t = (v_t)_w + [(v_t)_{t.e.} - (v_t)_w] \exp \frac{S_{t.e.} - S}{\ell_w \delta_{t.e.}} \quad (13)$$

where  $\ell_w = 20$ ,  $(v_t)_{t.e.}$  is the eddy viscosity at the trailing edge computed from its value on the airfoil and the expression for  $(v_t)_w$  is derived from the formula for the eddy viscosity in the far wake and is given by

$$(v_t)_w = 0.064 \int_0^{\delta} (u_{te} - u_t) dy \quad (14)$$

### 2.3 Stability/transition method

In order to determine the onset of the transition location, the saddle-point method of Cebeci and Stewartson<sup>12-13</sup> is used to solve the three-dimensional compressible linear stability equations.

The method has been extensively applied to the calculation of transition on wings at transonic and supersonic cruise conditions<sup>13</sup> and is used here. See Refs. 6 and 7 for details.

### 2.4 Viscous effects in inviscid method and drag

Once the boundary layer solution is known, the viscous effects must be modeled in the inviscid method to obtain the velocity distribution corrected for viscous effects. A wall-bounded viscous flow can be replaced by a fictitious inviscid flow either by displacing the surface of a quantity  $\Delta$  or by applying a blowing velocity at the wall such that the velocity

components at the edge of the boundary layer are equal for the real and fictitious flows.

The resulting equations for the displacement surface,  $\Delta$ , and blowing velocity,  $v_b$ , distributions on the wing and in the wake are

$$\frac{\partial}{\partial x}(h_2 u_e \sin \theta(\Delta - \delta_x^*)) + \frac{\partial}{\partial z}(h_1 w_e \sin \theta(\Delta - \delta_z^*)) = 0 \quad (15)$$

$$v_b = \frac{1}{h_1 h_2 \sin \theta} \left[ \frac{\partial}{\partial x}(h_2 u_e \sin \theta \delta_x^*) + \frac{\partial}{\partial z}(h_1 w_e \sin \theta \delta_z^*) \right] \quad (16)$$

The blowing velocity is used as the boundary condition on the panels and the pressure distribution is calculated at the displacement surface. Also, the Kutta condition is satisfied at the trailing edge of the displacement surface. A new inviscid solution is obtained and input to the boundary layer method. The process is repeated until convergence is reached.

The drag coefficient is calculated in the far field by adding induced drag and profile drag. The latter is computed following the procedure used to derive the Squire-Young formula.<sup>14</sup> Here however, instead of using the trailing edge values for  $u_e$ ,  $H_e$ , etc., the far wake values (computed several chords downstream) are used (e.g. for taking into account the effect a deployed flap has on the wake stemming from the main element).

### 3.0 Modified C.S. model for three-dimensional separated flows

To test the accuracy of the extension of the two-dimensional CS turbulence model to three-dimensional flows, calculated velocity profiles obtained with the original and the modified CS models are compared with wind tunnel measurements.<sup>15,16</sup> The experimental setup simulates the flow over an infinite swept wing with a pressure gradient leading to boundary layer separation (see Fig. 3).

To compare the calculated results with the experimental data, the infinite swept wing boundary layer equations are solved. Here, since the displacement thickness distributions ( $\delta_x^*$  and  $\delta_z^*$ ) are known, the boundary layer equations are solved in inverse mode using  $\delta_x^*$  and  $\delta_z^*$  as boundary conditions. Calculations are performed with the original and the modified CS models. Fig. 4 shows a comparison between the calculated and measured total edge

velocity ( $u_{te}$ ) distribution. As flow separation approaches, the results obtained with the original CS model begin to deviate while those obtained with the modified CS model agree well with data. Fig. 5 shows the variation of total skin friction coefficient. Agreement between data and calculations is excellent.

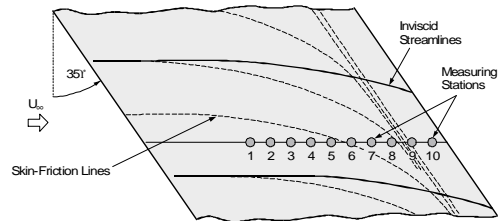


Fig. 3. NLR experiment: external streamlines and skin friction lines

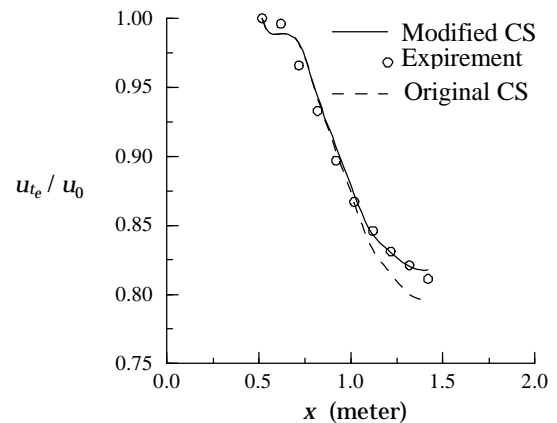


Fig. 4. Total edge velocity

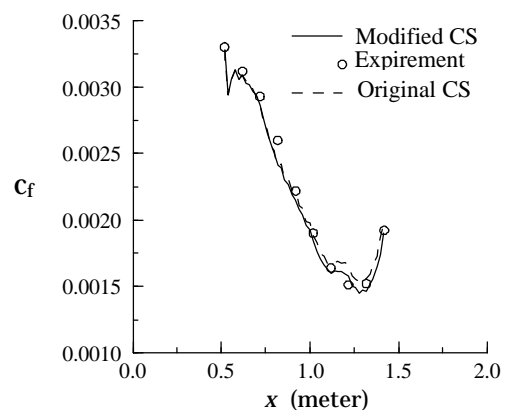
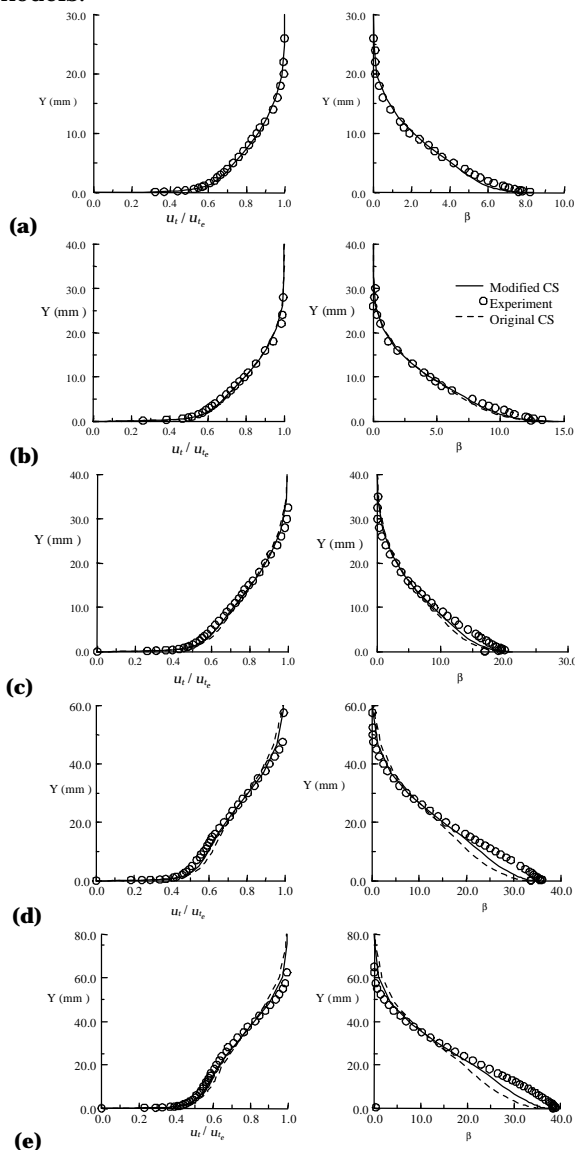


Fig. 5. Total skin friction coefficient distribution

Fig. 6 shows a comparison between the calculated and measured total velocity and crossflow angle distribution across the boundary layer. Up to station 5, the original and modified CS models give essentially the same results. The total velocity is well predicted, and except near the wall, the calculated crossflow angle agrees well with data. As separation approaches, the

modified CS model performs better than the original CS. At station 9, the total velocity profile computed with the modified CS model agrees well with experimental data, even if some rather large discrepancy between measured and calculated crossflow angle is observed near the wall.

More results and comparisons with experimental data can be found in Ref. 17. It is interesting to note that the results obtained with the modified CS model are in better agreement with data than those obtained using a  $k-\epsilon$  model<sup>18</sup>, and are approximately the same as those obtained with various Reynolds Stress models.<sup>18</sup>



**Fig. 6. Total velocity and crossflow angle across the boundary layer at (a)  $x = 820$  mm (station # 4), (b)  $x = 920$  mm (# 5), (c)  $x = 1020$  mm (# 6), (d)  $x = 1220$  mm (# 8), and (e)  $x = 1320$  mm (# 9).**

#### 4.0 Linearization of turbulence terms

As mentioned in Sect. 2, the discretization of the boundary layer equations at a given point ( $x, z$ ) leads to a set of non-linear difference equations which are linearized with Newton's method. The linearization of the laminar flow equations is straightforward but the expressions used to model the Reynolds stresses present difficulties when applied to the turbulent flow equations. Therefore, it is common practice not to linearize the turbulence quantities thus reducing convergence rates, or more dangerously, adding to the possibility of oscillations which might prevent convergence.

In Ref. 6, several levels of linearization are investigated. For conciseness, only a summary is included here. The results are presented in terms of maximum change of  $V$  (derivative of  $U (\equiv u / u_o)$  with respect to  $\eta$ , where  $\eta$  is defined in Eq. (6)) during Newton iterations. The derivatives of the crossflow profile exhibit a similar behavior.<sup>6</sup>

A sample of results is presented here for a wing with  $30^\circ$  sweep with an Eppler 387 airfoil cross-section at  $Re = 200,000$  and  $\alpha = 4^\circ$ . Two  $x$ -locations at  $\eta_b = 0.26$  are selected,  $x/c = 0.65$  and  $0.98$ , identified by  $NX = 50$  and  $75$ , respectively. Fig. 7 shows the variation of the skin friction coefficient in the  $x$ -direction at this wing cross-section. For  $NX = 50$ , the flow is turbulent and separated and for  $NX = 65$ , the flow is turbulent and attached. Fig. 8 shows the maximum residual in  $V$  across the boundary layer with Newton iterations without and with the linearization restricted to the term inside the brackets in Eq. (9), i.e. partial inner layer linearization only.

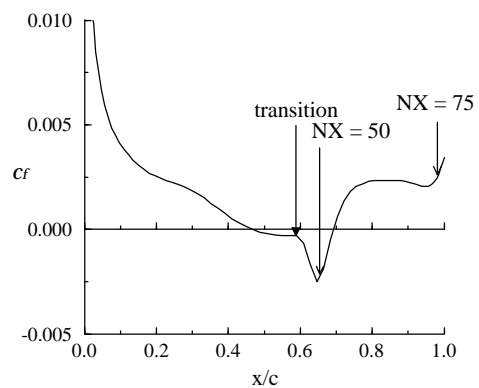


**Fig. 7. Skin friction coefficient distribution and selected points for the convergence study.**

Drastic improvements in convergence rates are observed, in particular for the case of separated flow. No significant added improvement is reported in Ref. 6 when the outer layer (integral in Eq. (10)) and other terms (i.e.  $\alpha$  in Eq. (10)) are included in the linearization. These results suggest that it is desirable to partially linearize the inner layer ( $\ell$  was not linearized) to increase numerical solution speed and stability, especially since it does not add to the complexity and cost of the solution of the linear system. However, including the outer layer and the wake in the linearization increases the cost associated with the solution of the linear system<sup>6</sup> but might prove beneficial for flows with higher pressure gradients, particularly in the wake region when a large region of separated flow is present. More studies are warranted to investigate this point.

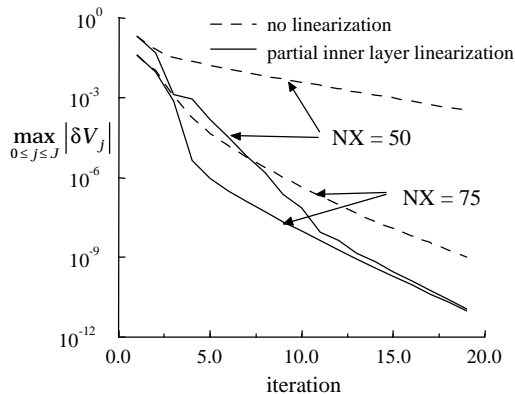


**Fig. 8. Partial linearization of turbulence terms and convergence acceleration.**

### **5.0 Single-element wing**

The method is applied here to a single-element wing tested by Lovell<sup>19</sup> at a mean aerodynamic chord Reynolds number of  $1.35 \times 10^6$ . The wing has an aspect ratio of 8.35, a quarter chord sweep angle of  $28^\circ$ , and a taper ratio of 0.35. The semi-span of the model is 1.074 m.

The measurements conducted by Lovell for the single wing were performed both with free and fixed transition. In order to eliminate possible differences due to changes in transition location, calculations are performed with fixed transition, i.e.  $(x/c)_{tr} = 0.0$  for the upper surface and  $(x/c)_{tr} = 0.1$  for the lower surface. In the experiments, transition was set by using a series of 0.5mm diameter wires positioned streamwise round the leading edge from 10%

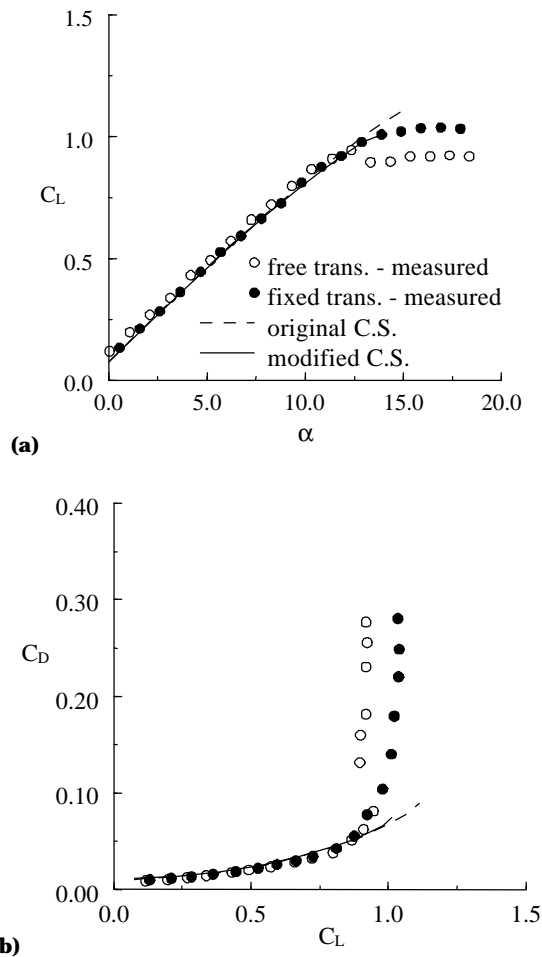
chord on the upper surface to 10% chord on the lower surface. Ten wires were equally spaced across each half wing. Measurements showed that the maximum lift coefficient with fixed transition is higher than that with free transition. Lovell noted, however, that “a larger portion is probably caused by the tendency of the streamwise wires to act as vortex generators.” Also, at post stall conditions, the flow becomes largely unsteady and only average measurements were reported. Therefore, near maximum lift, calculated results with fixed transition should be compared with free transition measurements. Both sets of experimental data are shown in Fig. 9.

Fig. 9a shows the lift coefficient variation with angle of attack. Results show that with the original C.S. model, the lift coefficient keeps on increasing past the measured stall angle (around  $12^\circ$  with free transition). For the modified C.S. model, agreement between measured and calculated lift coefficient is excellent up to  $14^\circ$ . At  $15^\circ$ , boundary layer calculations at  $\eta_b = 0.7$  did not converge in the wake due to the large separated flow region.

Fig. 9b shows the corresponding drag coefficient. Again, agreement between data and calculations is quite satisfactory up to stall. Fig. 10 shows the evolution near stall of the calculated streamwise displacement thickness at the trailing edge of the wing. Going from  $\alpha = 13$  to  $14^\circ$ , the maximum displacement thickness is multiplied by a factor of 1.6, indicating that the wing is at or very close to stall conditions. Fig. 11 shows the corresponding location of flow separation along the span. As can be seen in Figs. 10 and 11, and as expected for a swept non-twisted wing, stall is initiated near the tip, at about  $\eta_b = 0.7 - 0.8$ . In such a situation, the quasi-three-dimensional flow approximation in the viscous calculations might be questionable. For a real aircraft, however, in order to prevent a sudden roll, wings are usually designed to stall first inboard where the quasi three-dimensional flow approximation would be more appropriate, even at stall conditions.

Work is currently in progress to solve the numerical problems encountered at stall and compute some post stall behavior. Since the modified C.S. model yields improvements over

the original C.S model near stall conditions, it will be used in the remaining sections.



**Fig. 9. Single wing: effect of turbulence model on (a) lift and (b) drag coefficients**

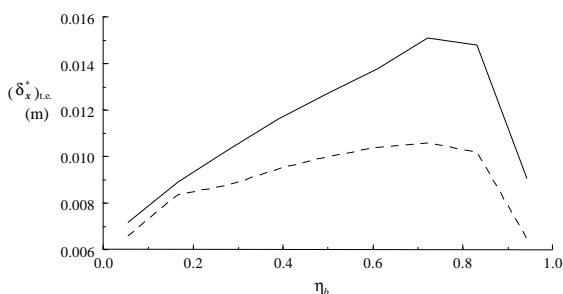


**Fig. 10. Displacement thickness distribution at the wing trailing edge near stall**

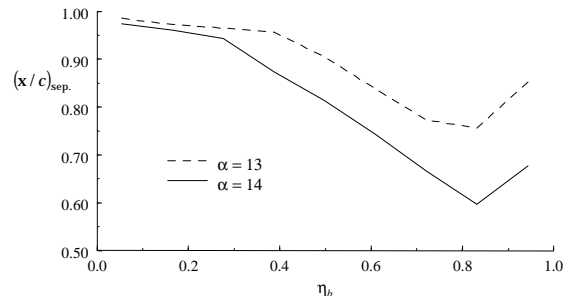


**Fig. 11. Extent of separated flow near stall conditions**

The effect of transition location was also studied in Ref. 6. It was shown that transition plays a role for drag predictions, even if this role is less pronounced than for two-dimensional flows. In fact, the need for calculating transition location depends on the goal set forth. For accurate boundary layer parameter predictions, transition should be calculated.<sup>5</sup> Except near stall, at moderate and high Reynolds numbers, lift predictions are relatively insensitive to transition location. For the purpose of predicting the drag coefficient reasonably well, it might be sufficient to perform transition calculations for a limited number of angles of attack, focusing on the lower surface of the wing, in particular to determine if cross-flow disturbances cause transition. For the upper surface, at moderate to high angles of attack, transition would usually occur either some short distance upstream of the pressure peak (if due to cross-flow disturbances) or some short distance downstream of the pressure peak (if due to Tollmien-Schlichting waves), so that setting it at the pressure peak should yield satisfactory results.

For more accurate drag predictions, transition should be calculated. Also, possible attachment line transition and/or relaminarization should also be included and could be incorporated into the present method.

### **6.0 Three-dimensional high lift systems**

In this section, the method is applied to wings with flap and slat deployed and results are compared with experimental data.<sup>19</sup> Fig. 12 shows a typical panel distribution (with every other panel and the wakes omitted for clarity). In light of the results Ref.6, calculations are performed with transition on the upper surface fixed at the leading edge. Also, in order to be able to retract the various elements, surface irregularities (coves) are present on the lower

surface of the slat (if deployed) and of the main element (if the flap is deployed). The coves are seen in Fig. 13 where each element is shown. For the present calculations, these coves are faired and transition is assumed to take place at the location of the start of the fairing.

Detailed results are presented for a wing-flap configuration and a slat-wing-flap configuration. A summary of the results is then presented for a total of five high lift configurations.

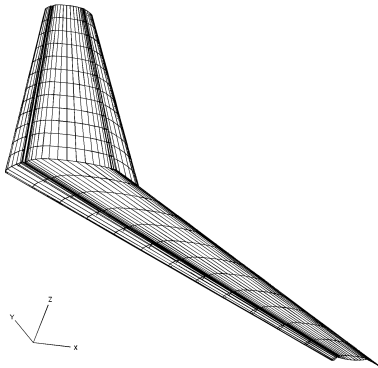


**Fig. 12. Multi-element wing paneling with slat and flap deployed at 25° -wakes omitted**

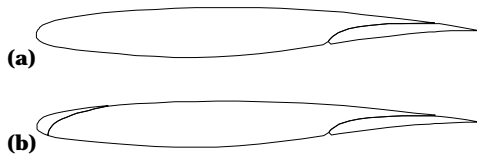


**Fig. 13. Elements of the high lift system (a) main element and flap when slat is retracted and (b) slat, main element, and flap**

The cross-section of the wing-flap configuration with the flap deflected at 25° is shown in Fig. 14a. The lift coefficient variation with angle of attack and the drag polar are also shown in Fig. 14. The inviscid lift coefficient is indicated to show how the introduction of the viscous effects allows for a better prediction of the lift curve. However, the lift coefficient is slightly over-predicted, possibly due to a merging of the main element wake with the boundary layer developing on the flap upper surface. Also, several reasons can be advanced to explain why stall is not predicted by the calculation method. One of them is based on prior two-dimensional experience. Even if the freestream Mach number is low (around 0.2), very high pressure peaks occur at the leading edge of the main element and can lead to locally

supersonic flow. Also, a separation bubble is usually present near the pressure peak with transition taking place in that bubble. The stronger pressure gradient when the flap is deployed makes this separation bubble even shorter than for a single wing. The combination of these two phenomena – taking place on such a short distance – makes accurate calculations in that region a challenging task. Fig. 14c shows that the drag coefficient is accurately predicted.

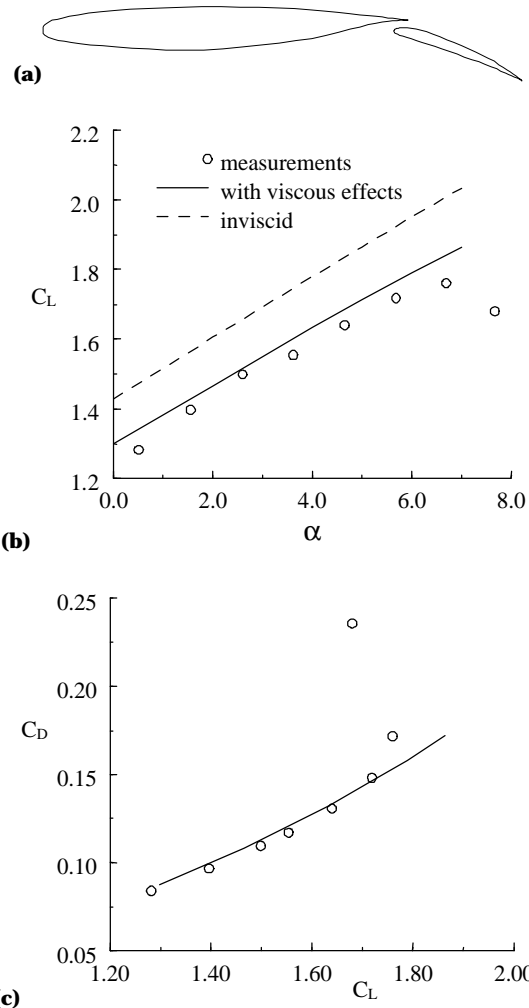


**Fig. 14. RAE wing with slat retracted and flap deflected at 25°, (a) wing cross-section, (b) lift coefficient, and (c) drag coefficient.**

Results are now presented in Fig. 15 for the configuration of the previous paragraph with the slat deflected at 25°. Again, the inviscid lift coefficient is indicated to show how the introduction of the viscous effects allows obtaining improved predictions of lift and drag coefficients. The discrepancies can be partly explained by the merging of the shear layers which was not accounted for. In addition, the

large recirculating flow region in the slat cove – larger at low angles of incidence– was removed with the fairing and may contribute to the disagreement at low angles of attack. Cove calculations, however, could be incorporated by extending the method previously discussed<sup>1</sup> to three-dimensional flows. The wake shape, prescribed in the inviscid method, may also be at the source of the discrepancy.

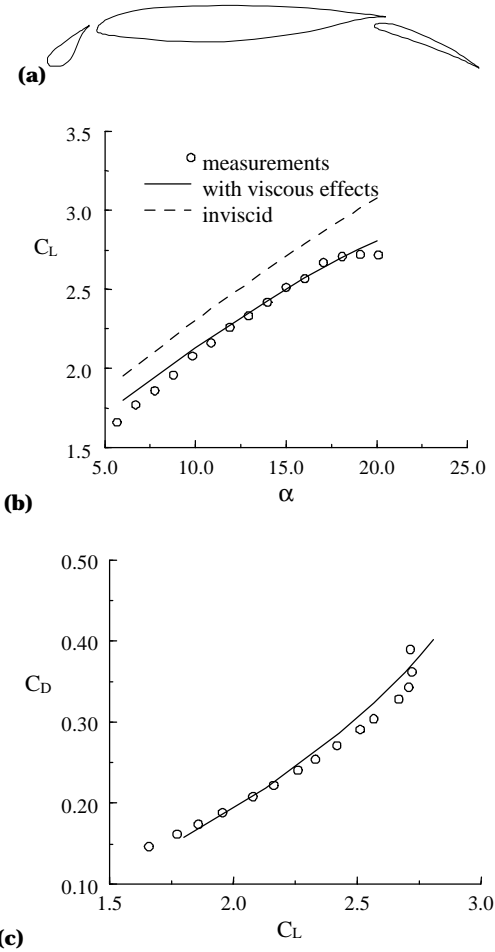


**Fig. 15. RAE wing with both slat and flap deflected at 25°, (a) wing cross-section, (b) lift coefficient, and (c) drag coefficient.**

Stall is not captured for the configurations tested. However, it is worthwhile to note that, at the present time, the reliable prediction of stall for slat-wing-flap configurations still offers significant challenges for two-dimensional flows. Unlike for single element and wing-flap configurations, stall can occur without flow separation on the main element but may instead be due to a sudden increase of the wake thickness thus reducing the circulation on the

entire configuration. Therefore, the present results should be viewed as quite satisfactory.

Fig. 16 shows a summary of the predicted effects of extending various high lift components and compares the results with measurements. Results for the clean wing (all high lift systems retracted), for two wing-flap configurations (full-span flap deployed at 10° and 25°, respectively), and for two slat-wing-flap configurations (full-span slat deployed at 25° with the two flap settings) are presented.

Overall, except for stall conditions, the increments in lift and changes in drag due to the deployment of high lift systems are well predicted. Further investigations are warranted to determine what influence the various approximations (quasi three-dimensional boundary layer, coves, shear layer merging, wake shape, compressibility, turbulence model) may have on solution accuracy.

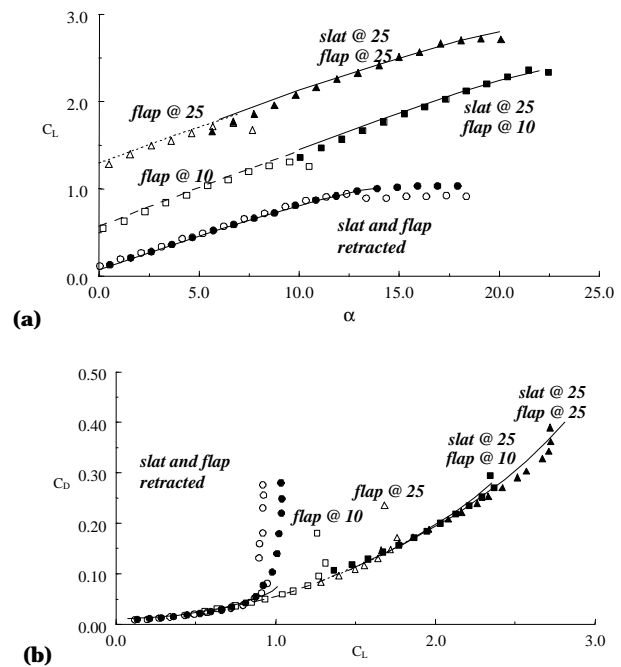


**Fig. 16. Performance of high lift devices; (a) lift and (b) drag coefficients.**

### 7.0 Concluding remarks

A method based on a stability-transition-interactive-boundary-layer approach for predicting the flow about single and multi-element wings with large regions of separated flow is described. The extension to three-dimensional flows of the modified CS model is validated for flows with regions of flow

separation. Agreement between measured and calculated velocity profiles is much better with the modified CS model than with the original version. The partial linearization of the turbulence terms is shown to yield significant improvements in boundary layer solution convergence rates leading to increased speed and robustness. The calculation method is then applied to three-dimensional high lift systems. Results are first presented for a single-element wing. Agreement between calculated and measured lift and drag coefficients is excellent up to stall conditions. It is shown that the modifications to the original CS model yield better agreement with data near stall conditions. Results for multi-element wings with slat and flap deployed demonstrate the ability of the method to predict lift and drag coefficients accurately. In this case, however, stall is not predicted as accurately as in two-dimensional flows. Work is in progress to address this issue. The need for a larger experimental database available to CFD developers in the area of three-dimensional high lift configurations is stressed. Overall, results demonstrate the potential for using the method as a practical and efficient design tool for high lift applications.

### **References**

1. T. Cebeci, E. Besnard and H.H. Chen, "Calculation of Multielement Airfoil Flows, Including Flap Wells," AIAA Paper No. 96-0056, Jan. 1996.
2. B.G. Arlinger et al., "Reynolds- and Mach number Effects and 2D-3D Correlation Based on Measurements and Computed Results for the Garteur Take-off Configuration," *Proceedings of High Lift and Separation Control*, Royal Aeronautical Society, London, March 1995.
3. N.B. Nield, "An Overview of the 777 High Lift Aerodynamic Design," *Proceedings of High Lift and Separation Control Conference*, Royal Aeronautical Society, March 1995.
4. E. Besnard, A. Schmitz, E. Boscher, N. Garcia, and T. Cebeci, "Two-dimensional Aircraft High-Lift System Design and Optimization," AIAA Paper 98-0123, Jan. 98.
5. E. Besnard, T. Vermeersch, G. Reboul, A. Schmitz, and T. Cebeci, "Prediction of Wing Flows with Separation," AIAA Paper No. 98-0404, Jan. 1998.
6. E. Besnard, "Prediction of High Lift Flows with Separation," Ph.D. Dissertation, Claremont Graduate University and California State University, Long Beach, May 1998.
7. T. Cebeci, *An Engineering Approach to the Calculation of Aerodynamic Flows*, to be published, 1999.
8. J.L. Hess, "Calculation of Potential Flows About Arbitrary Three-dimensional Lifting Bodies," MDC Report No. J5679-01, 1972.
9. R.L. Panton, *Incompressible Flow*, John Wiley & Sons, 1984.
10. A.E.P. Veldman, 'New quasi-simultaneous method to calculate interacting boundary layers.' *AIAA J.*, **19**, p.769, 1981.
11. T. Cebeci and K.C. Chang, "An Improved Cebeci-Smith Turbulence Model for Boundary-Layer and Navier-Stokes Methods," *Proceedings of the 20<sup>th</sup> ICAS/AIAA Aircraft System Conference*, Sept. 1996.
12. Cebeci T. and Stewartson K., "Stability and Transition in Three-dimensional Flows," *AIAA J.* **18**, p. 398, 1980.
13. Cebeci T., Chen H.H., and Arnal D., Natural Transition in Compressible Flows on Wings: Spatial Theory and Experiment," AIAA Paper No. 94-0824, Jan. 1994.
14. H.B. Squire and A.D. Young, 'The calculation of profile drag of aerofoils.' ARC RM 1838, 1938
15. B. van den Berg and A. Elsenaar, "Measurements in three-dimensional incompressible turbulent boundary layer in an adverse pressure gradient under infinite swept wing conditions," Technical Report NLR TR 72092 U, N.L.R., 1972.
16. A. Elsenaar and S.H. Boelsma, "Measurements of the Reynolds Stress Tensor in a Three-Dimensional Turbulent Boundary Layer under Infinite Swept Wing Conditions," NLR TR-74095 U, N.L.R., 1974.
17. T. Cebeci, "Extension and evaluation of the modified C.S. model for separated flows by using an inverse boundary-layer method and

its application to Navier-Stokes methods.”  
Paper in preparation.

18. P. Malecki, “Etude de modèles de turbulence pour les couches limites tridimensionnelles,” Thèse de l’Ecole Nationale Supérieure de l’Aéronautique et de l’Espace, Toulouse, 1994.
19. D. A. Lovell, “A Wind-Tunnel Investigation of the Effects of Flap Span and Deflection Angle, Wing Planform and a Body on the High-Lift Performance of a 28° Swept Wing,” R.A.E., C.P. No. 1372, Farnborough, U.K.1977.